Venus Gravity:

180th Degree and Order Model

A.S. KONOPLIV, W.B. BANERDT, and W.L. SJOGREN

Jet Propulsion Laboratory, California Institute of Technology,
4800 Oak Grove Drive, Pasadena, California 91109

Alex Konopliv: Tel: (818) 354-6105. Fax: (818) 393-6388
E-mail: ask@krait.jpl.nasa.gov

Bruce Banerdt: Tel: (818) 354-5413. Fax: (818) 393-9226
E-mail:william.b.banerdt@jpl.nasa.gov

Bill Sjogren: Tel: (818) 354-4868. Fax: (818) 393-6388
E-mail: wls@nomad.jpl.nasa.gov

Submitted to Icarus, Geodynamics of Venus Special Issue - 23 pages, 9 figures, 4 tables
Key words: gravity, spherical harmonics, Doppler

Running Title: Venus Gravity: 180th Degree and Order Model.

Corresponding Author:
Alex Konopliv
M.S. 301-125J
Jet Propulsion Laboratory
California Institute of Technology
4800 Oak Grove Drive
Pasadena, CA 91109

ABSTRACT

The Magellan Doppler radiometric tracking data provides unprecedented precision for spacecraft based gravity measurements with the maximum resolution approaching spherical harmonic degree and order 180 in selected equatorial regions. Determining a gravity field to degree 180 with a complete covariance containing the correlations between all the spherical harmonic coefficients (a 4.5 GB binary file for the triangular matrix) would be an extensive computational task even on the JPL/Caltech supercomputer that we used. Instead we determined a gravity field complete to degree and order 180 but in three separate steps. This gravity solution (MGNP180U) was determined first to degree and order 120 with a complete covariance for all the coefficients to degree 120. The second step solved for the coefficients from degree 116 to 155 only and the third step from degree 154 to 180. MGNP180U shows substantial improvement over previous solutions (up to and including MGNP120PSAAP, Konopliv et al, 1996a) especially in the medium to shorter wavelengths (harmonic degree 80 and greater). The rms magnitude power in the spectrum has increased as well as the correlations with topography. The amplitudes of various features have increased substantially (up to 33%, e.g., Bell Regio and Maat Mons). This will allow for better investigation of lithospheric modeling for shorter wavelength features such as coronae, volcanoesi, and impact basins.

Introduction

Two spacecraft orbiters, Magellan and Pioneer Venus Orbiter (Pioneer 12 or PVO), provide nearly a global gravity data set for Venus. Together they have been used to solve for a 180th degree and order spherical harmonic gravity field of Venus and additional parameters such as the ephemeris of Venus with respect to the Earth and the pole and rotation rate of Venus. The Venusian Love number results have been previously reported (Konopliv and Yoder, 1996b) and indicate that the Venus core is liquid.

The initial spherical harmonic determinations of the Venus gravity field were from the PVO tracking data set. Ananda et al (1980) determined a field to degree and order six and Williams et al (1983) to degree and order seven. Mottinger et al (1985) extended the harmonic solution to degree and order ten by using only high-altitude periapse (about 1000 km) data from PVO, and Bills et al (1987) solved for a degree and order 18 field by combining the high-altitude data with low-altitude data arcs. In support of the Magellan Navigation effort, McNamee et al (1992) reprocessed the low-altitude PVO data to produce a 21st degree and order model. Using the low and high altitude PVO data sets, Nerem et al (1993) determined a 50th degree and order field.

In September of 1990, Magellan was inserted into orbit about Venus. During the first three cycles (one cycle or eight months provided complete global longitudinal coverage), the high gain antenna was pointed toward Venus to acquire Synthetic Aperture Radar (SAR) images and no Doppler tracking was obtained within 30 minutes of periapse (periapse altitude was at 250 km). McNamee et al (1993) produced another 21st degree and order field incorporating Magellan cycle 1 and 2 high-altitude data with the PVO data. With the Magellan data from the gravity campaign in cycles 4, 5, and 6, the resolution of the gravity field greatly increased. Cycle 4 began in September 1992 after a maneuver to lower periapse to 170 km and tracking was obtained through periapse. Konopliv et al (1993) produced a 60th degree and order model (PMGN60C) by combining the PVO data with four months of Magellan data (or about one-half of longitude coverage from cycle 4). After

Magellan successfully aerobraked into a near circular orbit in August of 1993, Konopliv and Sjogren (1994a) produced another 60th degree and order model (MGNP60FSAAP) incorporating much of the near circular orbit data, and Konopliv et al (1994b) produced a 75th degree and order model (MGNP75ISAAP) with all the Magellan gravity data.

After the 75th degree solution, the gravity computations were moved from our computer workstations to the JPL Cray T3D and more recently the Caltech/JPL HP SPP2000 supercomputer. Since then resolution has continued to increase with a 90th degree and order field (MGNP90LSAAP, Sjogren, et al, 1997, Konopliv and Sjogren, 1996c) and a 120th degree and order field (MGNP120PSAAP, Konopliv, et al, 1996a). For the 120th degree field, all the LOS (line-of-sight) accelerations remaining in the residuals were also delivered to the Geosciences Node of the Planetary Data Systems (PDS), at Washington University (St. Louis, MO).. This included all the Doppler X-band data for cycles 4, 5, and 6. Most recently, a 155th degree and order field (MGNP155S, Konopliv and Sjogren, 1997) was presented. Although similar in development, that solution has a slightly tighter constraint than the solution (MGNP180U) in this paper. The harmonic coefficients of both fields are also available from the lead author or from the Geosciences Node of the PDS.

The spherical harmonic gravity fields mentioned above are dynamically determined. All the forces on the spacecraft are modeled and their effect on the spacecraft's orbit is estimated from the tracking data. Thus gravity coefficients are determined by short term acceleration visible in the residuals and the longer term effect on the orbit. Other methods using the LOS data have been used to determine the gravity field both regionally (Barriot et al, 1997, McKenzie and Nimmo, 1997) and globally (Kaula, 1996). These methods are geometric in that they compute the spacecraft velocity in the line-of sight direction from the Earth to Venus and then downward continue the accelerations to the surface of Venus. The effect of the spacecraft accelerations on the spacecraft orbit are neglected and if the long to medium wavelength gravity signature has been removed this is a good approximation. For

instance, our solutions for the spacecraft positions change by 300 meters when using a 120th degree truncation of the 180th degree field. This is not a source of error in reducing the spacecraft line-of-sight accelerations since it is below the resolution of the gravity field (which is 100 km for a 180th degree field), but it does indicate that there is still a significant amount of orbit or dynamical information beyond degree 120 in the tracking data. With a full 180th degree gravity field, the orbit uncertainty is about 100 to 200 meters mostly in the alongtrack direction. In our analysis special care was given to the gravity constraint in that it is spatially different depending on the strength of the data, but detailed investigations of each region was not done. Careful LOS analysis most likely will result in improved high frequency gravity.

Gravity Data

The gravity measurements used for Venus gravity field determination are two-way (station-to-spacecraft-to-station) coherent Doppler tracking of the PVO and Magellan spacecraft acquired at the Deep Space Network (DSN) complexes at Goldstone, California; Madrid, Spain; and Canberra, Australia. The PVO spacecraft operated at the S-band frequency of 2.2 GHz. The Magellan spacecraft had an S-band transponder with an X to S-band uplink converter and S to X-band downlink converter. The resulting system had either an X-band or S-band uplink and an S-band and/or X-band downlink. The X-band uplink and X-band downlink (8.43 GHz) provided the highest resolution gravity data because of reduced charged particle effects on the X-band signal. All two-way Magellan data were processed beginning with the gravity data of cycle 4.

PVO was inserted into orbit about Venus on December 4, 1978 and provided several years of low-altitude periapse data (150 to 170 km) until July of 1980 after which no maneuvers were performed to maintain a low periapse altitude. The data sample rate at periapse is 5 seconds. Data are included in the solution until November of 1980, where periapse altitude reached 400 km due to solar perturbations on the orbit. About one year of high altitude data (1000 km periapse altitude) beginning in November 1981 are included in

the gravity solution. Konopliv and Sjogren (1996c) and Sjogren et al, 1997 give a extensive description of the PVO and Magellan data and their orbits.

Cycle four for Magellan began on September 15, 1992 and continued to May 24, 1993. During the complete cycle, there were no periapse altitude adjustments and the altitude varied between 185 and 165 km. Magellan was tracked through periapse with a two-second sample time, but for the spherical harmonic gravity solutions, the sample time was compressed to 10 seconds. With a periapse velocity of 8.5 km/s, 10 second samples provide one plus samples per half wavelength of a 180th degree and order field. This is undersampled but is alleviated with multiple longitudinal coverage (multiple cycles) and orbit groundtrack separation of 20 km for cycle 4 and 10 km for cycles 5 and 6. The 10 second sample time was chosen to reduce the computational time required to generate the solution. There are 770,000 10-second observations (both X and S-band) for cycle four.

At the end of May, 1993, Magellan periapse was lowered deep into the atmosphere to begin aerobraking. Over the next several months to early August, the atmospheric drag on the spacecraft changed the orbit to nearly circular to provide much lower altitude gravity tracking at the higher latitudes. From August 6, 1993 (August 17 for beginning of X-band) to October 10, 1994, Magellan was tracked in this nearly circular orbit with apoapse altitude varying from 600 km to 350 km and periapse altitude from 155 km to 220 km. The same compression time of 10 seconds is used for the post-aerobraking data and amounts to 1,230,000 observations. The velocity of the Magellan spacecraft in the nearly circular orbit is about 7 km/s, providing an alongtrack sample every 70 km.

The PVO and Magellan data are divided into data arcs where the time span of the arc is typically one week for PVO (one orbit per day) and three days for Magellan. The arcs for PVO are the same as our previous work but the Magellan arc lengths were increased by a factor of three beginning with the 120th degree and greater solutions (Konopliv et al, 1996a). Thus the Magellan arcs contain about 24 orbits per arc for cycle 4 and about 48

orbit per arc for cycles 5 and 6. For each arc the solution for the spacecraft position and velocity is independent of the other arcs.

Gravity Modeling

The PVO and Magellan Doppler observations were processed using JPL's Orbit Determination Program (ODP) (see Moyer, 1971); the software set used at JPL for navigation of all planetary spacecraft. The ODP was modified for use on the Caltech/JPL HP SPP2000 supercomputer and it estimates the spacecraft state and other parameters using a square root information weighted least squares filter (see Lawson and Hanson, 1995; Bierman, 1977) in the coordinate system defined by the Earth's mean equator at the epoch of J2000. The parameters that are estimated consist of arc dependent variables (spacecraft state, etc.) that are determined separately for each data arc and global variables (harmonic coefficients, etc.) that are common to all data arcs. The global parameters are determined with a technique described by Kaula(1966) and Ellis (1980) that merges only the global parameter portion of the square root information arrays from all the arcs of PVO and Magellan, but is equivalent to solving for the global parameters plus arc dependent parameters of all arcs.

Initially, we converge the data arcs by estimating only the local variables using the nominal values for the global variables. For each data arc the local variables estimated are the spacecraft state, three solar pressure coefficients, a factor for the Venus albedo, the base density for each periapse passage through the atmosphere, the lift-to-drag coefficient for the low-altitude PVO orbits, velocity vector increments for the momentum wheel desaturations and star calibrations of Magellan, acceleration vectors for the hides of Magellan, and a UT1 bias for the PVO arcs. The a priori uncertainties for the spacecraft state are large (20 km). The a priori base density uncertainties for the PVO orbits are large but are more tightly constrained for Magellan (within 2×10^{-12} gm/cm^3 of the VIRA atmosphere model, Keating et al, 1985). The a priori on the Magellan desaturations are 0.5 mm/s and for the star

calibrations are 0.3 mm/s. The hides are constrained to 10^{-10} km/s^2. For a more detailed discussion of the force and observational modeling, see Konopliv and Sjogren, 1996c.

The observations of each arc are weighted according to data root mean square (rms) of that arc with a separate rms for each tracking station pass and with the rms including corrections for the count times of the observations. The actual data weight used is the rms multiplied by a factor of two with an additional correction factor for the observation elevation. Since the PVO and Magellan orbits are nearly polar, the groundtracks converge near the pole and the observations become more dense. For this reason, the observation sigma is adjusted for latitude ϕ ($\sigma_{new} = \sigma_{old} * \cos^{-1/2}\phi$). Using this weighting scheme results in roughly correct accuracies for the longer to medium wavelength coefficients. The formal sigmas for the low degree terms need to be increased by a factor of 2 or three to be realistic but the sigmas of the high degree terms are too large and need to be scaled down. This is due to the nongaussian or red noise characteristic of the Doppler data (Woo, 1975).

The gravitational potential of Venus is modeled by a spherical harmonic expansion with normalized coefficients ($\bar{C}_{nm}$, $\bar{S}_{nm}$) and is given by

$$U = \frac{GM}{r} + \frac{GM}{r} \sum_{n=2}^{\infty} \sum_{m=0}^{n} \left(\frac{a_e}{r}\right)^n \bar{P}_{nm}(\sin\phi) \left[\bar{C}_{nm}\cos m\lambda + \bar{S}_{nm}\sin m\lambda\right]$$

where n is the degree and m is the order, $\bar{P}_{nm}$ are the fully normalized associated Legendre polynomials, a_e is the reference radius of Venus (6051.0 km for our models), ϕ is the latitude, and λ is the longitude. The normalized coefficients are related to the unnormalized by (see Kaula, 1966)

$$(\bar{C}_{nm}\ ;\ \bar{S}_{nm}) = \left[\frac{(n+m)!}{(2-\delta_{0m})(2n+1)(n-m)!}\right]^{1/2} (C_{nm}\ ;\ S_{nm})$$

where δ_{0m} is the Kronecker delta function and $\overline{C}_{n0} = -\overline{J}_n$. The harmonic coefficients of degree one are fixed to zero since the origin of the coordinate system is chosen to be the center of mass of the body. The body-fixed coordinate system is nominally given by the 1991 IAU values (Davies et al, 1992a, 1992b) for Venus pole position and rotation rate.

Determining a gravity field to degree and order 180 with a complete covariance containing the correlations between all the spherical harmonic coefficients would be an extensive task even on the JPL/Caltech supercomputer. The covariance would be a 4.5 GB binary file for the triangular matrix.. Instead we determined a gravity field complete to degree and order 180 but in three separate steps. First, using a 120th degree and order field (MGNP120PSAAP) as the nominal, a new 120th degree and order field was determined (named MGNP120USAAP). The global variables in this case are the harmonic coefficients (about 15,000 parameters), the gravitational mass of Venus, the right ascension and declination of the pole of Venus and rotation rate of Venus. Using the full unconstrained covariance, a spatial a priori (described below) was applied to obtain the gravity solution. Using MGNP120USAAP as the nominal solution, the same local variables of each arc were redetermined. Then a new gravity field (MGNP155USAAP) was determined with the global variables being only the coefficients from degree 116 to degree 155 (about 11,000 parameters). In doing a subset of the coefficients, the correlations between all the gravity coefficients are lost but this saves much computational time (about a factor of 5). The constraint for the second set of coefficients is also a surface constraint as for the 120th solution. Again this process is repeated using MGNP155USAAP as the nominal solution and the coefficients from degree 154 to degree 180 (about 10,000 parameters) as the global variables to obtain the final solution MGNP180U. This time a power law or Kaula constraint ($\sim 1/n^2$) is applied that does not vary spatially to obtain those coefficients. For the last solution step (degrees 154 to 180), the power law constraint provided the smoothest spectral solution and so was the method of choice.

Gravity A Priori

Once all the global information is packed from all the data arcs, the gravity field is constrained with an a priori. The common method is to constrain each harmonic coefficient toward zero with an uncertainty given by the Kaula rule (Kaula, 1966) for that particular planet (used, for example, in Konopliv et al. 1993, Nerem et al. 1993, McNamee et al. 1993 and for the second and third steps of this solution). The Kaula rule for Venus is $1.2 \times 10^{-5} / n^2$ where n is the degree of the coefficient. Although for the constraint in the third step (degrees 154 to 180), a more relaxed Kaula rule of $4.0 \times 10^{-5} / n^2$ is applied to pull more information out of the data. This is due to the "red" noise characteristics of the Doppler data as mentioned above.

We outline below a second method that applies a spatially varying constraint based upon the data strength. These particular solutions are given the SAAP label, Surface Acceleration A Priori. This particular method given below was used beginning with Konopliv and Sjogren, 1996c or MGNP90LSAAP. It was also used for Mars in Konopliv and Sjogren (1995a). This is the a priori that is used in the first and second steps of determining the 180th degree field.

The a priori constraint applied for this gravity field evaluates the radial acceleration and its uncertainty on the reference sphere (i.e., $r = a_e$). At that surface, the radial acceleration (a_n) from all coefficients of degree n is given by

$$a_n = \frac{GM}{a_e^2} (n + 1) \sum_{m=0}^{n} \bar{P}_{nm}(\sin \phi) (\bar{C}_{nm} \cos m\lambda + \bar{S}_{nm} \sin m\lambda)$$

To create a profile of acceleration contributions versus degree, the rms of the acceleration a_n is obtained over the sphere. As a good approximation, the rms magnitude spectrum of the gravity coefficients follows the Kaula rule and is given by

$$\left[\frac{\sum_{m=0}^{n} (\overline{C}_{nm}^2 + \overline{S}_{nm}^2)}{2n+1} \right]^{1/2} = K/n^2$$

where K is the constant for the particular planet (1.2×10^{-5} for Venus). The expected acceleration profile is then given by (for $n >> 1$)

$$(a_n)_{rms} = \frac{GM}{a_e^2} K\sqrt{2/n}$$

which for Venus is

$$(a_n)_{rms} = 15 / \sqrt{n} \text{ milligals} \qquad (1)$$

This is the expected "signal" for the acceleration at each point on the surface of the reference sphere. The signal could also be determined empirically by taking the rms of a given gravity field over different regions. However, for this work, only one signal profile is used for all latitudes and longitudes.

The next task is to map the acceleration uncertainty at the surface into an uncertainty or "noise" profile showing the error in acceleration versus harmonic degree. The acceleration uncertainty from the summed contributions of all coefficients from degree 2 to n, $\sigma(a_{2,n})$, is given by

$$\sigma(a_{2,n}) = \frac{\partial a_{2,n}^T}{\partial \mathbf{G}_{2,n}} \mathbf{P}_{noap(2,n)} \frac{\partial a_{2,n}}{\partial \mathbf{G}_{2,n}}$$

where $\mathbf{G}_{2,n}$ is the vector of all normalized gravity coefficients from degree 2 to n and $\mathbf{P}_{noap(2,n)}$ is the corresponding covariance. The covariance of the coefficients from degree 2 to n is the covariance as if the higher degree coefficients (>n) are not estimated. Hence, it is a truncation, or submatrix, of the full 120th degree and order covariance without any constraint applied to the gravity field. The partial derivatives of the acceleration with respect to the coefficients of degree n and order m are functions of latitude and longitude and are given by

$$\frac{\partial a_{2,n}}{\partial \overline{C}_{nm}} = \frac{GM}{a_e^2} (n + 1) \overline{P}_{nm}(\sin \phi) \cos m\lambda$$

$$\frac{\partial a_{2,n}}{\partial \overline{S}_{nm}} = \frac{GM}{a_e^2} (n + 1) \overline{P}_{nm}(\sin \phi) \sin m\lambda$$

The uncertainty for the coefficients of degree n, $\sigma(a_n)$ is then given by the difference of the sum total error to degree n and the sum total error to degree n-1 as

$$\sigma(a_n) = \sigma(a_{2,n}) - \sigma(a_{2,n-1}) \qquad (2)$$

Figure 1 shows the expected acceleration profile from the signal due to the Kaula rule and the noise from covariance for Atalanta, the periapse region for Magellan cycle 4 (eastern Eistla Regio), and the gap in Magellan cycle 5 data in the southern hemisphere (160°E to 220°E, 30°S to 80°S). The crossing point of the Kaula signal with the acceleration uncertainty is called the degree strength of the gravity field for that particular latitude and longitude. For degrees greater than the degree strength, the "noise" in the data

exceeds the "signal." Based upon the Kaula rule, the degree strengths for Atalanta, Eistla, and the southern gap are 62, 104, and 40, respectively. Figure 2 displays the spatial distribution of degree strength on a global scale. The maximum degree strength is greater than harmonic degree 100 near the low-altitude periapse locations, although the actual degree strength is greater because of the overly pessimistic data weight for the high frequency terms. Johnson et al, 1997, looking at the coherence of track-to-track Doppler residuals obtains resolution of the gravity data as high as degree and order 140. However, our value for the minimum degree strength of 35 south of eastern Aphrodite Terra is near the true value.

The basic idea of the gravity constraint method is to constrain the "noise" of the gravity field to zero with some uncertainty when the "noise" exceeds the "signal." The acceleration at the surface from all harmonic coefficients greater than or equal to the degree strength is constrained to zero with an uncertainty approximately equal to the expected signal at the degree strength. This amounts to generating observations over the entire surface of the sphere based upon the degree strength at each latitude and longitude. An observation ($a_{D,120}$) for degree strength D is

$$a_{D,120} = \frac{GM}{a_e^2} \sum_{n=D}^{120} \sum_{m=0}^{n} (n+1)\, \overline{P}_{nm}(\sin\phi)\, (\overline{C}_{nm}\cos m\lambda + \overline{S}_{nm}\sin m\lambda)$$

and the linearized observation equation is given by (Bierman, 1977)

$$z_i = \mathbf{A}_i\, \mathbf{x} + v_i$$

where z_i is the difference between the observed value (zero in this case) and the nominal value of the observation (the accumulated acceleration at the surface for degrees D to 120 from the a priori gravity), $\mathbf{A}_i$ is the row vector of observation partials (the partial of the

observation with respect to all the parameters being estimated), $\mathbf{x}$ is the vector of estimated parameters (differences in the gravity coefficients from the nominal gravity model), and v_i is the observation error. The partials $\mathbf{A}_i$ to construct the observation equation are

$$\mathbf{A}_i = \frac{\partial a_{D,120}}{\partial \mathbf{G}}$$

where $\mathbf{G}$ is the vector of all gravity coefficients. The elements of $\mathbf{A}_i$ for coefficients with degrees less than the degree strength D are zero and, otherwise, are as given above.

The observations are then merged with the unconstrained gravity square root information array using Householder transformations. In normal form, the constrained gravity estimate $\mathbf{x}$ is written as

$$\mathbf{x} = \left[\mathbf{P}_{noap}^{-1} + \mathbf{A}^T\mathbf{W}\mathbf{A}\right]^{-1} \left[\mathbf{P}_{noap}^{-1}\mathbf{x}_{noap} + \mathbf{A}^T\mathbf{W}\mathbf{z}\right]$$

where $\mathbf{P}_{noap}$ is the unconstrained covariance of the gravity coefficients, $\mathbf{A}$ is the matrix of observation partials with each row an observation, $\mathbf{W}$ is the diagonal weight matrix, $\mathbf{x}_{noap}$ is the unconstrained gravity estimate, and $\mathbf{z}$ is the vector of linearized observations. The new constrained covariance $\mathbf{P}$ is then

$$\mathbf{P} = \left[\mathbf{P}_{noap}^{-1} + \mathbf{A}^T\mathbf{W}\mathbf{A}\right]^{-1}$$

The observations should be spaced such that at least three observations are generated over the shortest harmonic wavelength. The weight used for an observation is then proportional to the area between observations and is approximately equal to the signal at the degree strength (i.e., 10 to 20 milligals). The observations are globally distributed on a rectangular grid of latitude and longitude with a spacing of one degree.

The main advantage of using this spatial constraint instead of a straight Kaula rule on the spectrum appears to be better determination of peak amplitudes. Since the well determined degrees are not constrained directly (only somewhat through correlations), the amplitudes (and coefficients) for those degrees are not biased toward zero. It is also flexible in allowing relaxation of selected regions for any reason, such as incorrect data weighting or a region exhibiting greater signal than the power rule. In general, there are only slight differences between the two constraint methods since Venus does not have strong local deviations from Kaula power spectrum. For Mars, the differences are more pronounced for the Tharsis region (Konopliv and Sjogren, 1995a).

Gravity Results

The 180th degree gravity field has about 33,000 coefficients resulting in near one-degree or 100 km resolution in selected periapse regions. Figure 3 shows the vertical acceleration on a reference sphere of 6051.0 km for two of these areas, the volcanic swells of Beta Regio and Atla Regio. The rift zone of Beta Regio at 280-285°E and 15-20°N and Maat Mons of Atla regio are the strongest high frequency signatures on Venus. The correlation with topography for the rift zone is greater than 0.6 for degrees greater than 150. In Figure 3b the largest gravity amplitude of over 500 milligals is evident for Maat Mons. The greatest changes in the gravity field versus the previous 120th degree solution MGNP120PSAAP are in the equatorial region from Atla Regio eastward to Beta Regio. This area shows a very strong high frequency gravity signature. In addition, there is a significant increase in correlation between the gravity and topography for the entire Ishtar Terra.

Whereas the high frequency information in the gravity is well represented by the free-air acceleration, as seen in Figure 3, the geoid better displays the long wavelength features of the MGNP180U solution (Figure 4). The rift-zone of Beta and Maat Mons are not as evident but Maat Mons still has the largest geoid value of 158 meters with Beta the next largest amplitude of over 110 meters and Maxwell Mons of over 90 meters. The

uncertainty in the geoid from the 120th degree covariance is less than one meter for the equatorial regions and up to four meters for the gap in cycle 5 and 6 data near Imdr (in the southern hemisphere south of Atla). The corresponding free-air uncertainties are 10 milligals in the better determined areas and up to 50 milligals in the cycle 5 and 6 gap.

The GM, second degree coefficients, and their formal sigmas are listed in Table 1 for various solutions that we have produced. The formal sigmas are typically too small and the current formal sigmas need to be increased by a factor of 3 to 5. Again, this is due to long wavelength solar plasma noise in the data. There is a significant change in the coefficients between the 90th and 120th degree solutions because of the increase in data arc length from one day to three days and improved the long wavelength information for the gravity field. The principal axes of inertia, which are determined from the second degree harmonics, are listed in Table 2. There is a consistent offset of the polar inertial axis from the rotational pole of 0.5 degrees for all the solutions and indicates a wobble of the Venus pole (Yoder and Ward, 1979).

The Venus pole and rotation rate solutions are given in Table 3. Increasing the formal statistic by a factor of three to more realistic levels, our pole solution is 272.743±0.006 for the right ascension, 67.156±0.006 for the declination, and 243.0200±0.0006 days for the rotation rate. Our rotation period solution is slightly longer than that determined by Davies et al (1992b) of 243.0185±0.0001. Both, however are consistently below the 1988 IAU value (243.025) based upon Earth radar measurements of Venus and more recent radar determinations by Slade et al (1990) of 243.022 ± 0.003.

The coefficients of the gravity field show considerably increased power in the high degree terms versus the previous 120th degree solution MGNP120PSAAP. Figure 5 shows the rms magnitude spectrum for the two solutions MGNP180U and MGNP120PSAAP along with the uncertainty in the spectrum for MGNP180U. In the MGNP120PSAAP solution there is a distinct change (a slight discontinuity) in the curve at degree 90. This is because the nominal field for the MGNP120PSAAP solution is a 90th

degree solution. The new solution (MGNP180U) which is a complete iteration on the first 120th degree coefficients, eliminates this discontinuity. However, the higher degree terms beyond degree 120 now show a slight discontinuity and some decreasing power. The break at 120th degree and order is due to solving for only a complete 120th degree and order solution in the first step of our method (i.e., the coefficients greater than 120 are decorrelated in the solution for coefficients less than 120). This slight shift at 120 could be removed by solving for a complete 180th degree solution in one step. The would provide the best possible solution but would require significantly more supercomputer time and the resulting covariance would be a cumbersome 4 GB in size.

The different steps in solving for a 180th degree field are also evident in the uncertainty or sigma curve in Figure 5. The second step (solving for degrees 116 to 155) causes the slight change at degree 116 and the third step (solving for degrees 154 to 180) causes the slight change at degree 154. But the uncertainties from all three steps match fairly well and so does the power in the coefficients.

Figure 6 shows the admittance of the three gravity fields MGNP180U (this paper), MGNP120PSAAP (Konopliv et al, 1996a), and MGNP60FSAAP (Konopliv et al, 1994) together with the theoretical admittance for Airy-type compensation at depths of 25, 50, 100, 200, and 300 km. The admittance has substantially increased from earlier work especially in the higher degrees. Results indicate globally averaged Airy compensation at depths of 25 to 50 km for harmonic degrees 40 to 100. Beyond degree 100, the reduction in global admittance is due to lack of global resolution in the Doppler tracking data.

In addition to the increase in power and admittance, the 180th degree solution also shows substantial increase in correlation with topography (the 360th degree model of Rappaport et al, 1998). Figure 7 shows the correlation of the gravity and topography harmonic coefficients with the new model showing an increase in correlation beginning near degree 70 and extending for the higher degree terms with large differences from degree 90 to 120. The correlations decrease to near zero at degree 180 indicating the loss of

gravity signal in the data. There is not much benefit in extending the solution beyond degree 180. Figure 8 shows the spatial correlation of the gravity with topography for the high frequency terms between degree 120 and 150. The geoid and topography height are computed and the correlated with a sliding 10 degree rectangular window. Correlations above 0.8 are evident near Beta Regio and near 0.8 for Atla Regio and eastward to Beta. Other areas that show high correlation are Ishtar Terra (0.5) and eastern Eistla Regio (0.5), the location of several large coronae of interest. Figure 9 shows the spatial correlation of the gravity with topography for the high frequency terms between degree 150 and 180. The rift-zone of Beta shows the greatest correlation (>0.6) with correlations greater than 0.4 for portions of Atla and eastern Eistla.

The correlations (both spectral and spatial) and the power in the rms spectrum are sensitive to the amount of constraint applied to the gravity solution. For the first step (i.e., to degree 120), the constraint was relaxed to allow near maximum correlations of gravity with topography both spatially and spectrally. Any further relaxation tended to decrease the correlations. So power in the spectrum (and thus admittance) could be increased further by relaxing the a priori constraint some more but only at the expense (i.e, reduction) of the correlations. In addition, further relaxation produced addition visible noise in the gravity field as shown by the free-air anomalies. For the degrees greater than 120, the a priori was applied to maximize only the spatial correlations (as given by Figures 8 and 9) near the high resolution regions such as Atla and Beta. Any relaxation beyond this did not improve the correlations for those areas and actually tended to decrease them. However, the spectral or global correlations (as given by Figure 7) were smaller as a result of using this a priori (probably from increased noise). A tighter constraint would give better spectral correlations but at the expense of reduced power (and admittance) and spatial correlations for Atla and Beta. Even with the relaxed a priori, the uncertainty in the admittance for degrees greater than 120 remains large. Depending on how willing one is to reduce the correlations, the admittance can be significantly increased. So caution is needed in interpreting the high

frequency admittance (> degree 120). Nevertheless, the new gravity field is much improved for investigating small scale features such as volcanoes and coronae as has been done, for example, by Simons et al (1997), McGovern et al (1997) and Smrekar and Stofan (1998).

Bearing these caveats in mind, it can be seen from Table 4 that this gravity model has had a substantial effect on the amplitudes of nearly all the major gravitational features on the planet, even though the broader field remains nearly unaffected. The largest changes with respect to the previous solution are at Bell Regio, Maat Mons, and Mead Crater, with increases of 32%, 32%, and 55%, respectively. Although much of this increase is due simply to the inclusion of the additional shorter wavelength power beyond l=120, an appreciable portion is derived from the extra power that has gone into degrees 80-120. Only Atalanta Planitia, Gula Mons, and Maxwell Montes are nearly unaltered, suggesting that there is little short-wavelength structure (which is the case for Atalanta) or that the support of the major topographic extent of these features is relatively deep.

The gravity resolution of this field (full wavelengths of ~200 km) begins to cover the wavelength region where geophysical models for the support of substantial individual anomalies (such as major volcanoes, large impact basins, etc.) tend to be most sensitive to variation of parameters such as lithospheric thickness. For example, the admittance function of a simple top-loaded flexure model changes from a higher flexure-dominated value to a lower buoyancy-dominated value at a wavelength about 8 times the lithosphere thickness, with the bulk of the change occurring over about a decade in wavelength. For thin lithosphere models, this is just within the high-degree end of this model. Thus we expect that the availability of MGNP180U should allow for better high-frequency modeling, especially in the Atla, Bell and Beta regions.

Acknowledgments

The HP SPP2000 Supercomputer used in this investigation was provided by funding from the NASA Offices of Mission to Planet Earth, Aeronautics, and Space

Science. The research described in this paper was carried out by the Jet Propulsion Laboratory, California Institute of Technology, under a contract with the National Aeronautics and Space Administration.

References

Ananda, M.P., W.L. Sjogren, R.J. Phillips, R.N. Wimberly, and B.G. Bills 1980. A Low-Order Global Gravity Field of Venus and Dynamical Implications. *J. Geophys. Res.* 85, 8303-8318.

Barriot, J.P., G. Balmino, and N. Vales 1997. Building reliable local modes of the Venus gravity field from the Cycles 5 and 6 of the Magellan LOS gravity data. *Geophys. Res. Lett.* 24, No. 21, pp. 477-480.

Bierman, G. J. 1977. *Factorization Methods for Discrete Sequential Estimation*, Academic Press, New York.

Bills, B.G., W.S. Kiefer, and R.L. Jones 1987. Venus Gravity: A Harmonic Analysis. *J. Geophys. Res.*, 92, 10335-10351.

Davies, M.E., V.K. Abalakin, A. Brahic, M. Bursa, B.H. Chovitz, J.H. Lieske, P.K. Seidelmann, A.T. Sinclair, and Y.S. Tjuflin 1992a. Report of the IAU/IAG/COSPAR Working Group on Cartographic Coordinates and Rotational Elements of the Planets and Satellites: 1991. *Celes. Mech. 53*, 377-397.

Davies, M.E., T.R. Colvin, P.G. Rogers, P.W. Chodas, W.L. Sjogren, E.L. Akim, V.A. Stepanyantz, Z.P. Vlasova, and A.I. Zakharov 1992b. The Rotation Period, Direction of the North Pole, and Geodetic Control Network of Venus. *J. Geophys. Res.*, 97, 13141-13151.

Ellis, J. 1980. Large Scale State Estimation Algorithms for DSN Tracking Station Location Determination. *J. Astronaut. Sci., 28,* 15-30.

Johnson, C.L., S.C. Solomon, D.T. Sandwell, M. Simons 1997. Global and Regional Resolution Analyses of Magellan Gravity Data and Comparisons with Current Gravity Models. Presented at Geodynamics of Venus: Evolution and Current State, AGU Chapman Conf., Sept. 4-6, Aspen, CO.

Kaula, W.M. 1966. *Theory of Satellite Geodesy*, Blaisdell, Waltham, MA.

Kaula, W.M. 1996. Regional Gravity Fields on Venus from Tracking of Magellan Cycles 5 and 6. *J. Geophys. Res. Planets*, 101, 4683-4690.

Keating, G.M., J.L. Bertaux, S.W. Bougher, T.E. Cravens, R.E. Dickinson, A.E. Hedin, V.A. Krasnopolsky, A.F. Nagy, J.Y. Nicholson III, L.J. Paxton, U. von Zahn 1985. Models of Venus Neutral Upper Atmosphere: Structure and Composition. *Adv. Space Res.* **5**, 117-171.

Konopliv, A. S., N. J. Borderies, P. W. Chodas, E. J. Christensen, W. L. Sjogren, B. G. Williams, G. Balmino, and J. P. Barriot 1993 Venus Gravity and Topography: 60th Degree and Order Model. *Geophys. Res. Lett.* 20, No. 21, pp. 2403-2406.

Konopliv, A. S., and W. L. Sjogren 1994a. Venus Spherical Harmonic Gravity Model to Degree and Order 60, *Icarus* 112, 42-54.

Konopliv, A. S., W. L. Sjogren, E. Graat, J. Arkani-Hamed 1994b. Venus Gravity Data Reduction. Presentation at Fall 1994 Meeting, American Geophysical Union, San Francisco, CA, December 5-9.

Konopliv, A.S., W.L. Sjogren, C.F. Yoder, and E. Carranza 1996a. Venus 120th Degree and Order Gravity Field. 1996 AGU Fall Meeting, San Francisco, CA.

Konopliv, A.S. and C.F. Yoder 1996b.Venusian k2 Tidal Love Number from Magellan and PVO Tracking Data. *Geophys. Res. Lett.*, Vol. 23, No 14, pp 1857-1860.

Konopliv, A.S. and W.L. Sjogren 1996c. Venus Gravity Handbook. JPL Publication 96-2, Jet Propulsion Laboratory, Pasadena, CA, January.

Konopliv, A.S. and W.L. Sjogren 1997. Venus 155th Degree and Order Gravity Field. Presented at Geodynamics of Venus: Evolution and Current State, AGU Chapman Conf., Sept. 4-6, Aspen, CO.

Lawson, C. L. and R. J. Hanson 1995. *Solving Least Squares Problems.* SIAM Classics in Applied Mathematics, Vol. 15, Society for Industrial and Applied Mathematics, Philadelphia.

McGovern, P.J., C.L. Johnson, S.C. Solomon, and M. Simons 1997. Estimates of elastic lithophere thickness beneath large volcanos and coronae on Venus from spatio-spectral localization of harmonic gravity and topography. Presented at Geodynamics of Venus: Evolution and Current State, AGU Chapman Conf., Sept. 4-6, Aspen, CO.

McKenzie, D. and F. Nimmo 1997. Elastic Thickness Estimates for Venus from Line of Sight Accelerations. *Icarus* 130, 198-216.

McNamee, J.B., G.R. Kronschnabl, S.K. Wong, and J.E. Ekelund 1992. A Gravity Field to Support Magellan Navigation and Science at Venus. *J. Astron. Sci.*, 40, 107-134.

McNamee, J.B., N.J. Borderies and W.L. Sjogren 1993. Venus: Global Gravity and Topography. *J. Geophys. Res. Planets*, 98, E5, 9113-9128.

Mottinger, N.A., W.L. Sjogren and B.G. Bills 1985. Venus Gravity: A Harmonic Analysis and Geophysical Implications. *J. Geophys. Res.* 90, 739-756.

Moyer, T. D. 1971. Mathematical Formulation of the Double-Precision Orbit Determination Program (DPODP). JPL Technical Report 32-1527. Jet Propulsion Laboratory, California Institute of Technology, Pasadena, CA.

Nerem, R.S., B.G. Bills and J.B. McNamee 1993. A High Resolution Gravity Model for Venus: GVM-1. *Geophys. Res. Lett.*, 20, 7, 599-602.

Rappaport, N. J., A.S. Konopliv, A.B. Kucinskas, P.G. Ford 1998. An Improved 360 Degree and Order Model of Venus Topography", *Icarus* (this issue).

Simons, M., S.C. Solomon, and B.H. Hager 1997. Localization of gravity and topography: Constraints on the tectonics and mantle dynamics of Venus. *Geophys. J. International* 131, 24-44.

Sjogren, W.L., W.B. Banerdt, P.W. Chodas, A.S. Konopliv, G. Balmino, J.P Barriot, T.R. Colvin, M.E. Davies, and J. Arkani-Hamed 1997. The Venus Gravity Field and Other Geodetic Parameters. *Venus II*, S.W. Bougher, D.M. Hunten, and R.J. Phillips (eds), U. of Arizona Press, 1125-1161.

Slade, M.A., S. Zohar, and R.F. Jurgens 1990. Venus: Improved Spin Vector from Goldstone Radar Observations. *Astron. J., 100,* 1369-1374.

Smrekar, S. and E. Stofan 1998. Evidence for Delamination of Corona-Dominated Topographic Rises on Venus. *Icarus* (this issue).

Williams, B.G., N.A. Mottinger, and N.D. Panagiotacopulos 1983. Venus Gravity Field: Pioneer Venus Orbiter Navigation Results. *Icarus* 56, 578-589.

Woo, R. 1975. Multifrequency Techniques for Studying Interplanetary Scintillations. *Astrophys. J.*, 201, 238-248.

Yoder, C.F., and W.R. Ward 1979. Does Venus Wobble?. *Astrophys. J.*, 233 L33-L37.

Coefficient	60x60[1]	90x90[2]	120x120[3]	180x180[4]
GM	324858.63 ±0.01	324858.601 ±0.007	324858.590 ±0.006	324858.592 ±0.006
$\overline{C}_{20} \times 10^7$	-19938±29	-19716±7	-19698±7	-19697±7
$\overline{C}_{21} \times 10^7$	247±27	290±5	267±4	268±4
$\overline{S}_{21} \times 10^7$	-7±27	143±5	138±4	132±4
$\overline{C}_{22} \times 10^7$	8344±34	8547±9	8600±10	8578±10
$\overline{S}_{22} \times 10^7$	-888±39	-999±9	-951±10	-955±10

Table 1: GM and normalized harmonic coefficients of degree two and formal sigmas for the following gravity models: (1) Konopliv and Sjogren, 1994a, MGNP60FSAAP (2) Konopliv and Sjogren, 1996c, MGNP90LSAAP (3) Konopliv et al, 1996a, MGNP120PSAAP and (4) this paper, MGNP180U.

Axes 1,2,3	Axes of inertia			
(deg)	60x60[1]	90x90[2]	120x120[3]	180x180[4]
Latitude	0.3	0.38	0.35	0.35
Longitude	-3.0	-3.33	-3.15	-3.17
Latitude	0.0	0.36	0.34	0.33
Longitude	87.0	86.67	86.85	86.83
Latitude	89.67	89.48	89.51	89.52
Longitude	-179.3	-139.87	-138.74	-139.69

Table 2: Orientation of Venus' principal axes of inertia for the following gravity models: (1) Konopliv and Sjogren, 1994a, MGNP60FSAAP (2) Konopliv and Sjogren, 1996c, MGNP90LSAAP (3) Konopliv et al, 1996a, MGNP120PSAAP and (4) this paper, MGNP180U.

Parameter	90x90[1]	120x120[2]	180x180[3]	Davies(1992b)
Pole Right Ascension (deg)	272.749 ±0.002	272.743 ±0.002	272.743 ±0.002	272.76 ±0.02
Pole Declination (deg)	67.160 ±0.001	67.156 ±0.001	67.156 ±0.001	67.16 ±0.01
Rotation Rate (days)	243.0194 ±0.0002	243.0201 ±0.0002	243.0200 ±0.0002	243.0185 ±0.0001

Table 3: Venus pole right ascension and declination in Earth-Mean-Equator of J2000, rotation rate, and formal sigmas for the following gravity models (1) Konopliv and Sjogren, 1996c, MGNP90LSAAP (2) Konopliv et al, 1996a, MGNP120PSAAP and (3) this paper, MGNP180U.

Feature	Longitude	Latitude	90x90[1]	120x120[2]	180x180[3]
Maxwell	4.5	63.5	244.7	249.4	268.2
Akna	-42.5	68.5	115.2	121.1	154.8
Freya	-23.5	73.5	126.3	128.1	150.1
Bell	46.0	29.0	126.3	165.3	218.8
Beta	-79.0	25.5	234.3	237.9	288.7
Gula	-2.0	22.0	138.3	135.3	138.3
Maat	195.0	1.0	356.4	401.5	535.0
Ozza	200.0	3.5	245.5	228.5	268.9
Nokomis	190.0	19.5	132.9	147.7	168.6
Sapas	188.0	8.5	157.5	174.1	210.6
Atalanta	164.5	62.5	-84.4	-84.5	-85.8
Mead	57.2	12.6	-49.7	-67.0	-103.9

Table 4: Gravity peaks in milligals at the surface for Venusian features of interest for the following gravity models (1) Konopliv and Sjogren, 1996c, MGNP90LSAAP (2) Konopliv et al, 1996a, MGNP120PSAAP and (3) this paper, MGNP180U.

Figure 1. Contribution of each harmonic degree to the amplitude of the radial acceleration at the refernce surface and the radial uncertainty. The expected acceleration amplitude or signal is given by equation (1), the Kaula rule for Venus, and is the same for all latitudes and longitudes. The uncertainties in the accelertion profiles, as given by equation (2) using the unconstrained covariance, are given for three different regions, Atalanta, eastern Eistla, and the area with the poorest data resolution (the southern data gap at 180°E and 60°S).

Figure 2. The degree strength for gravity field MGNP180U as determined from the unconstrained 120th degree and order covariance in the first of three steps in obtaining the full 180th degree solution. The contours are in harmonic degree and represent the degree where the contribution to the signal of that degree (based on the Kaula rule) is equal to the contribution to the uncertainty.

Figure 3. Free-air gravity at the reference surface for (a) Beta Regio and (b) Atla Regio. Gravity is displayed in contour lines every 20 milligals with positive contours as solid lines and negative as dashed. The topography (Rappaport et al, 1998) is displayed in color with the same resolution as the gravity field (harmonic coefficients to degree and order 180).

Figure 4. Geoid of the full MGNP180U gravity field with respect to the reference sphere. Contours are in 10 meter intervals.

Figure 5. RMS magnitude spectrun of the gravity fields MGNP180U (this paper) and MGNP120PSAAP (Konopliv et al, 1996a) and the error spectrum for MGNP180U. Also shown is the Kaula rule scaled for Venus ($1.2 \times 10^{-5}/n^2$).

Figure 6. Global admittance from gravity fields (1) MGNP180U, (2) MGNP120PSAAP, and (3) MGNP60FSAAP. Displayed as lines without symbols are theoretical admittances from Airy compensation at depths of 25, 50, 100, 200, and 300 km.

Figure 7. Correlation of gravity coefficients with topography coefficients from Rappaport et al, 1998. Correlations are shown for gravity fields MGNP120PSAAP (Konopliv et al, 1996a) and MGNP180U (this paper).

Figure 8. Spatial correlation of the geoid with topography height for coefficients from degrees 120 to 150 only. The contours are in intervals of 0.2 with the positive contour correlations shown with the darker solid lines and the zero and negative contours shown with the lighter dashed lines.

Figure 9. Spatial correlation of the geoid with topography height for coefficients from degrees 150 to 180 only. The contours are in intervals of 0.2 with the positive contour correlations shown with the darker solid lines and the zero and negative contours shown with the lighter dashed lines.

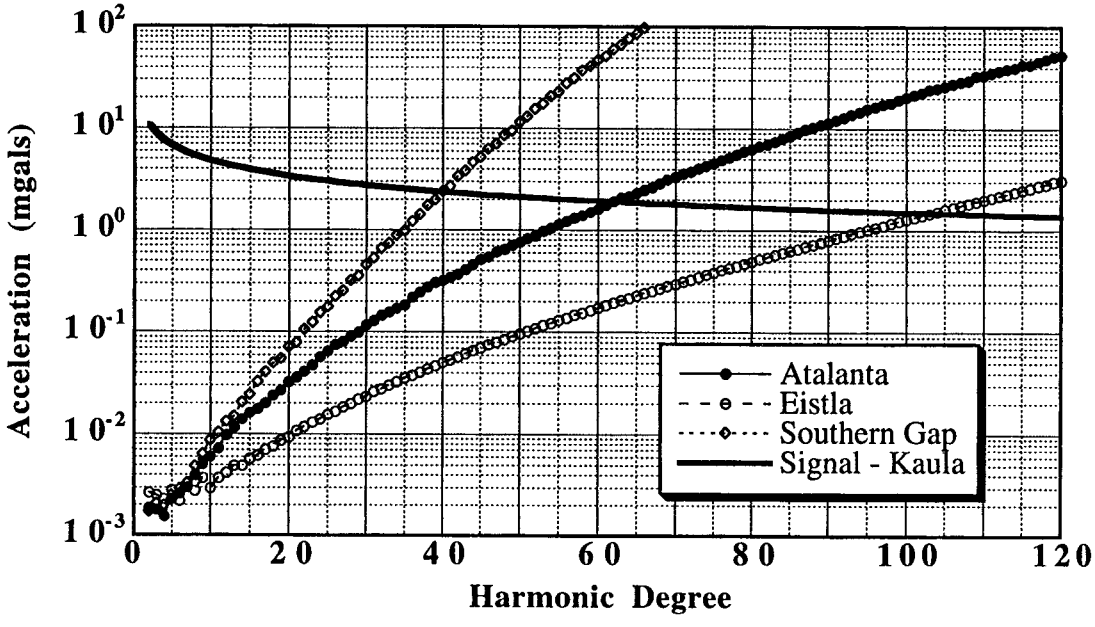
Acceleration (mgals)
1 0^2
1 0^1
1 0^0
1 0^-1
1 0^-2
1 0^-3
0
20
40
60
80
100
120
Harmonic Degree
Atalanta
Eistla
Southern Gap
Signal - Kaula

Fig. 1

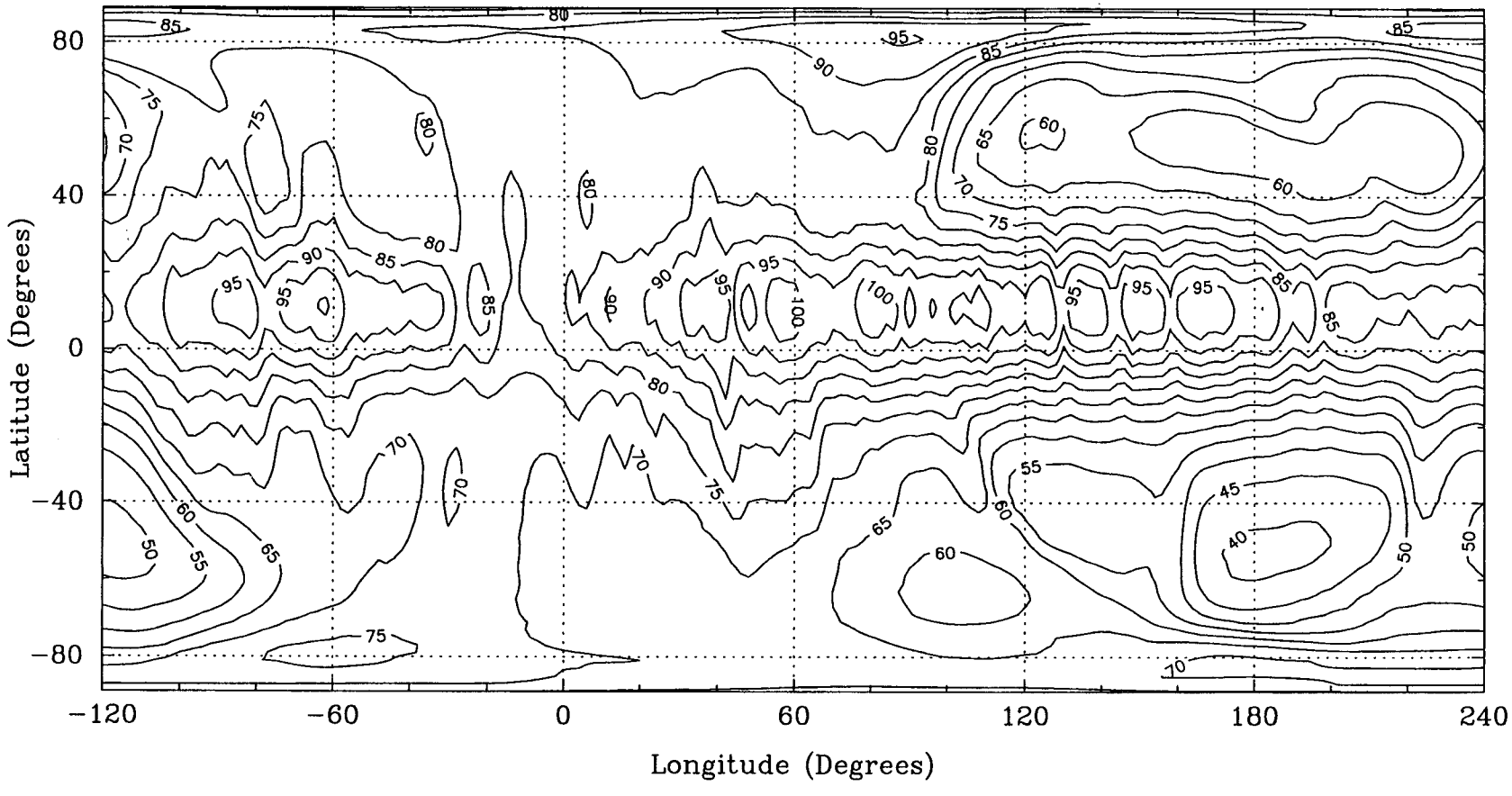
Latitude (Degrees)
80
40
0
−40
−80
−120
−60
0
60
120
180
240
Longitude (Degrees)

Fig. 2

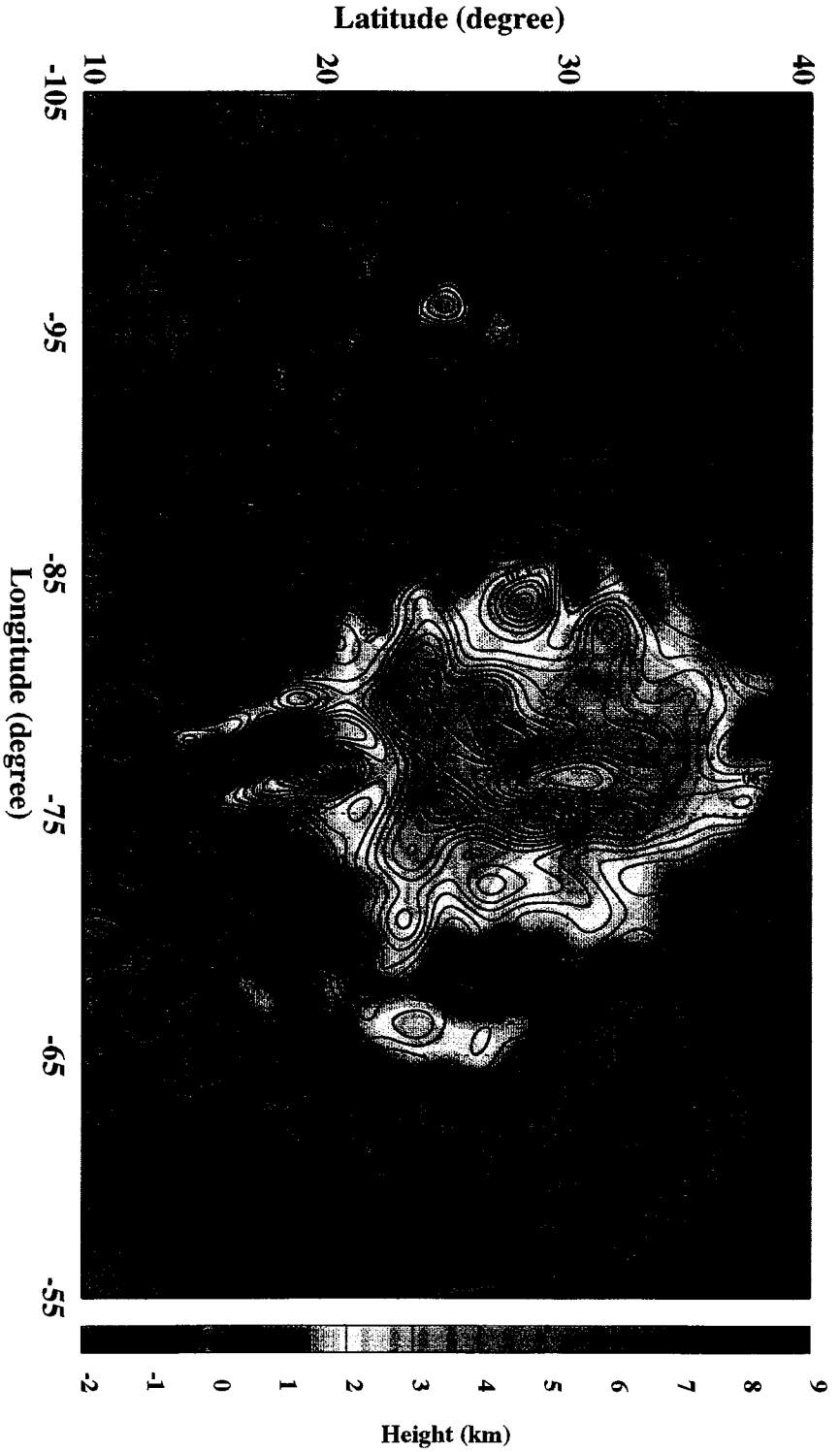
Latitude (degree)
10
20
30
40
Longitude (degree)
-105
-95
-85
-75
-65
-55
-2
-1
0
1
2
3
4
5
6
7
8
9
Height (km)

Fig 3a

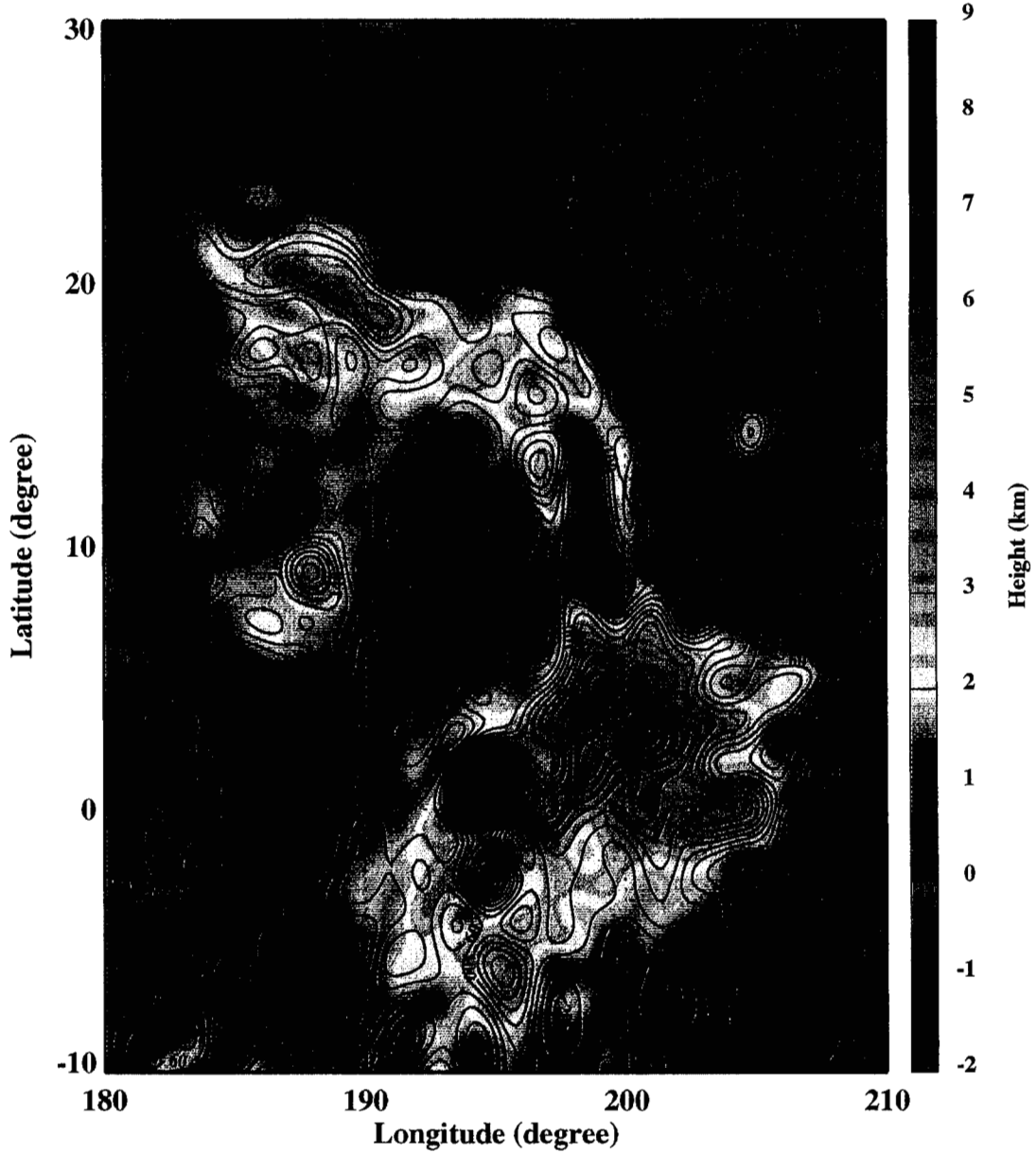
30
20
10
0
-10
Latitude (degree)
180
190
200
210
Longitude (degree)
9
8
7
6
5
4
3
2
1
0
-1
-2
Height (km)

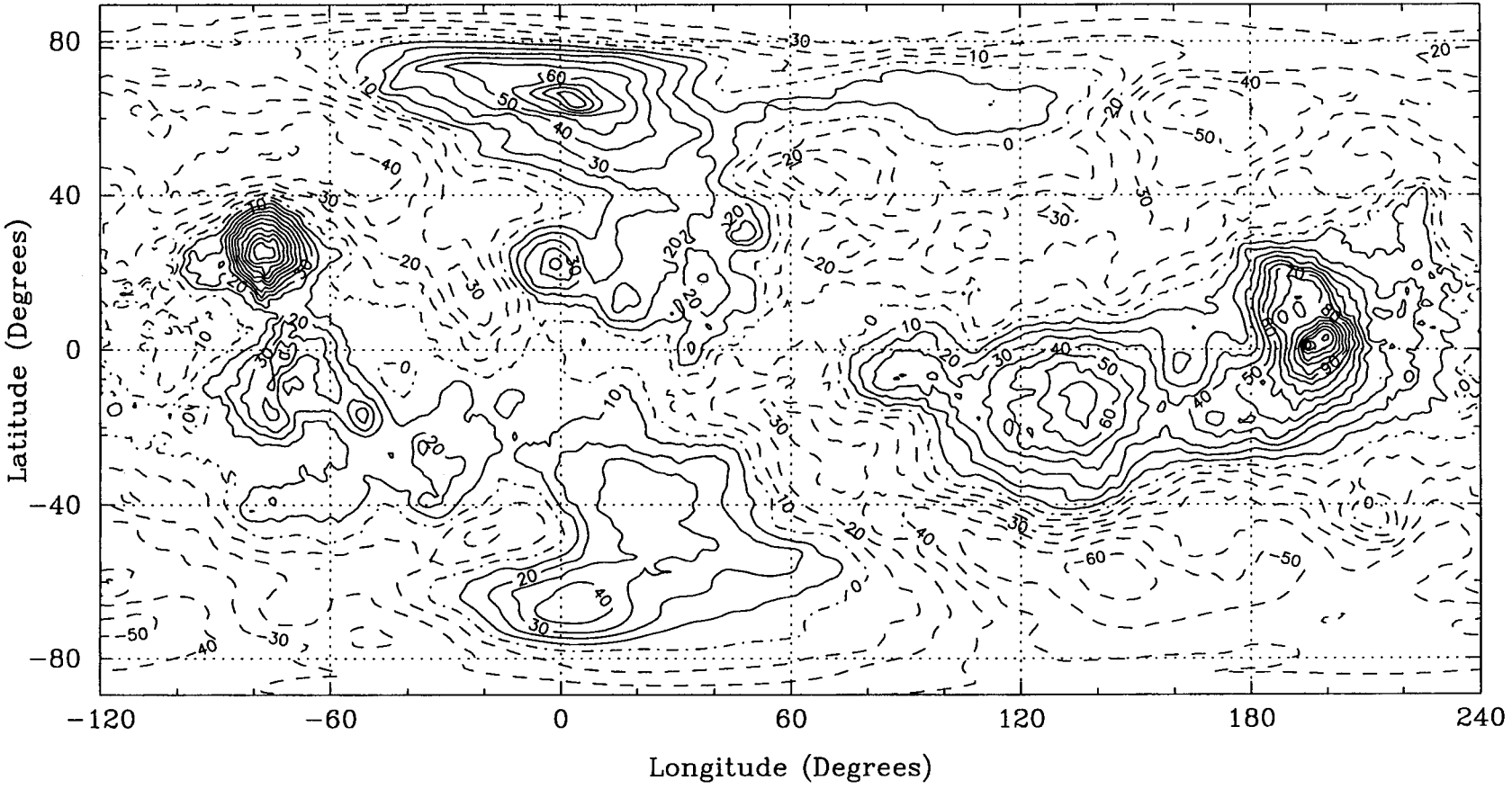
80
40
0
−40
−80
Latitude (Degrees)
−120
−60
0
60
120
180
240
Longitude (Degrees)

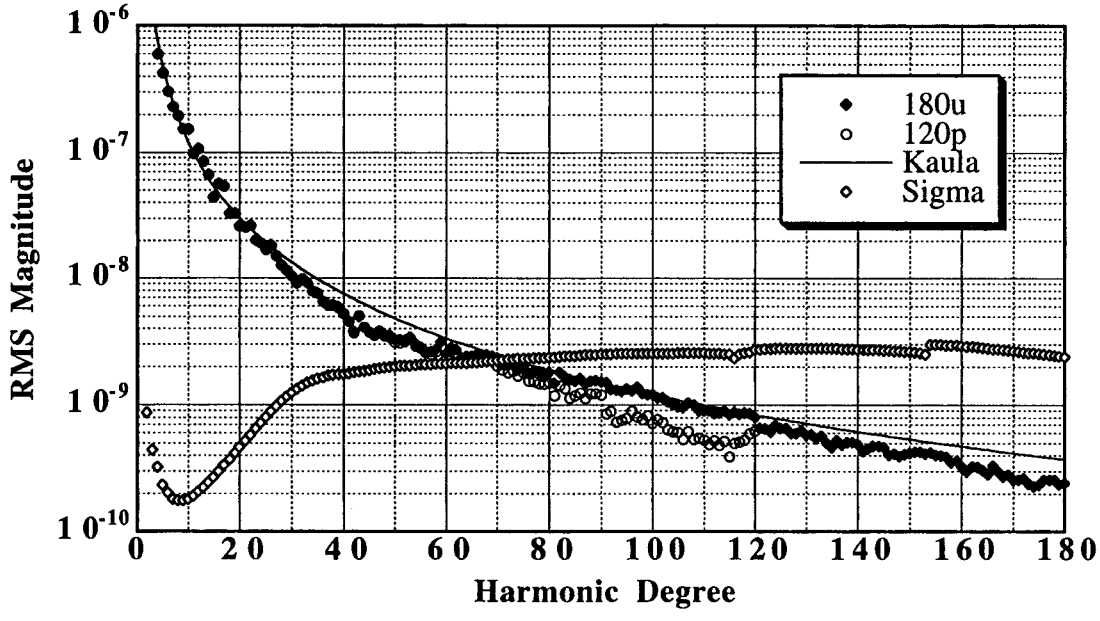
RMS Magnitude
10-6
10-7
10-8
10-9
10-10
0
20
40
60
80
100
120
140
160
180
Harmonic Degree
180u
120p
Kaula
Sigma

Fig. 5

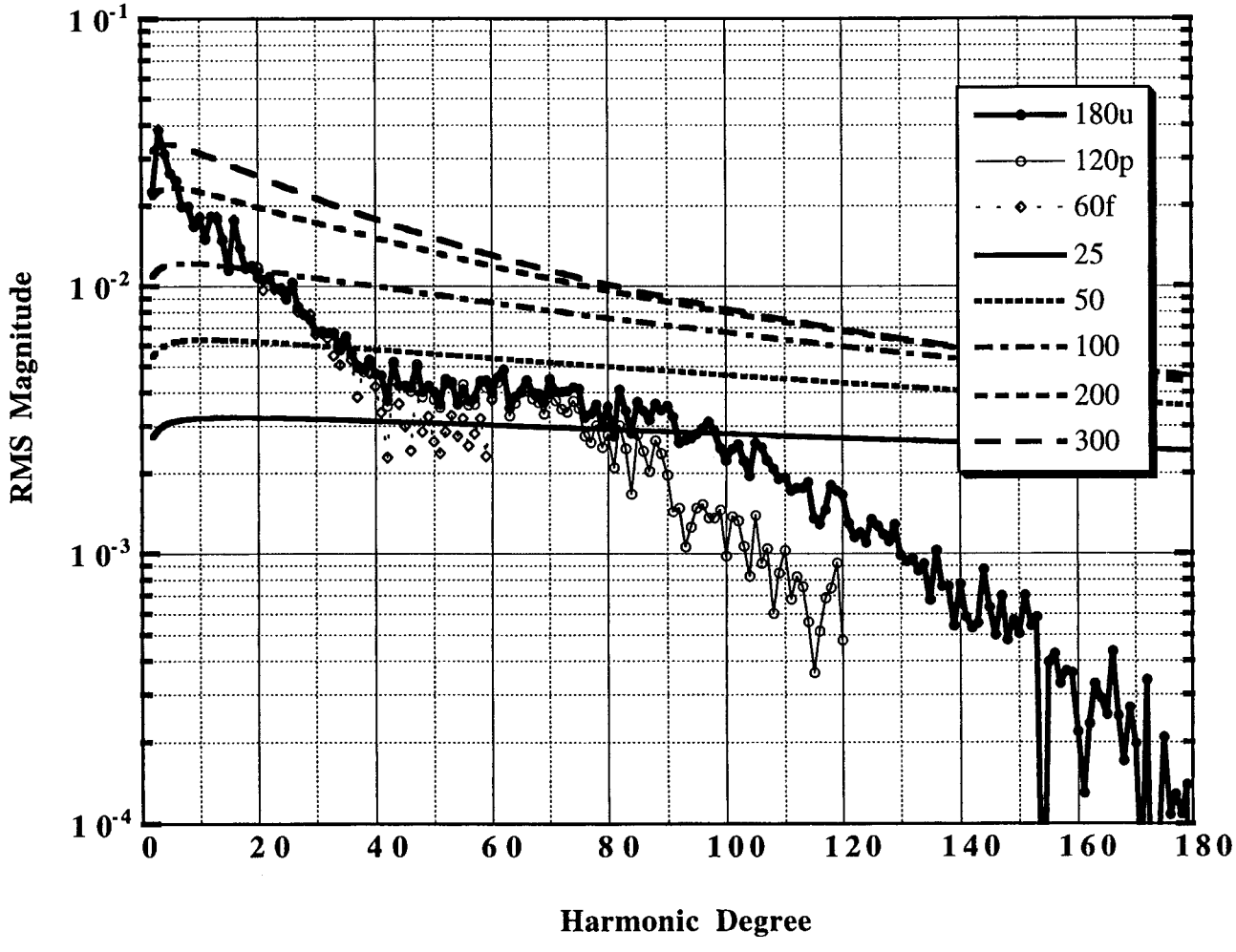
1 0-1
1 0-2
1 0-3
1 0-4
RMS Magnitude
0
20
40
60
80
100
120
140
160
180
Harmonic Degree
180u
120p
60f
25
50
100
200
300

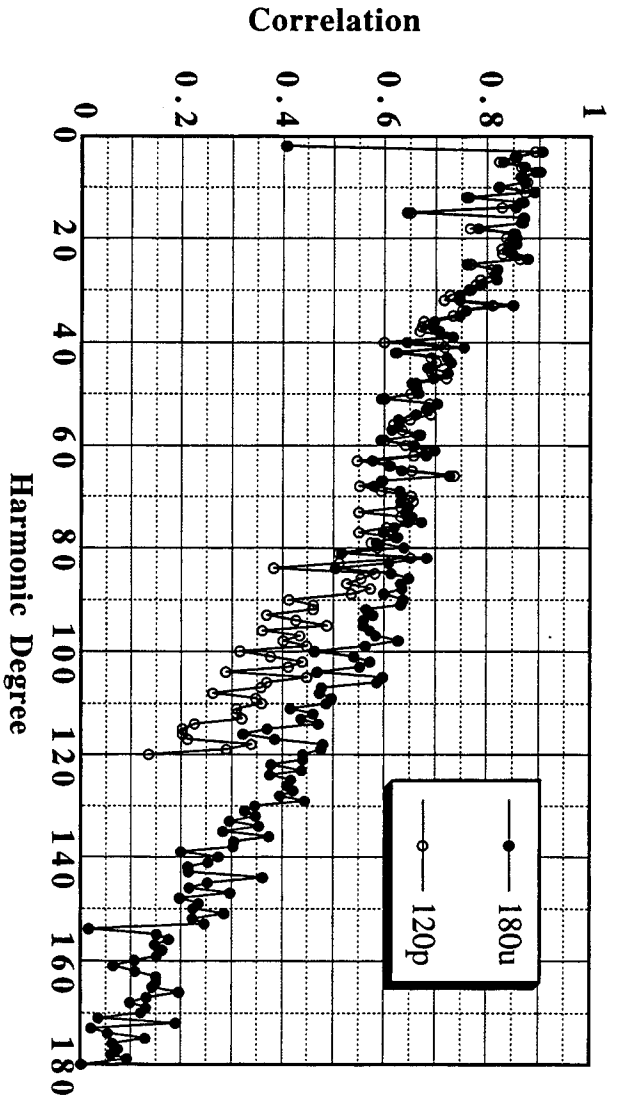
Correlation
1
0.8
0.6
0.4
0.2
0
0
20
40
60
80
100
120
140
160
180
Harmonic Degree
180u
120p

Fig 7

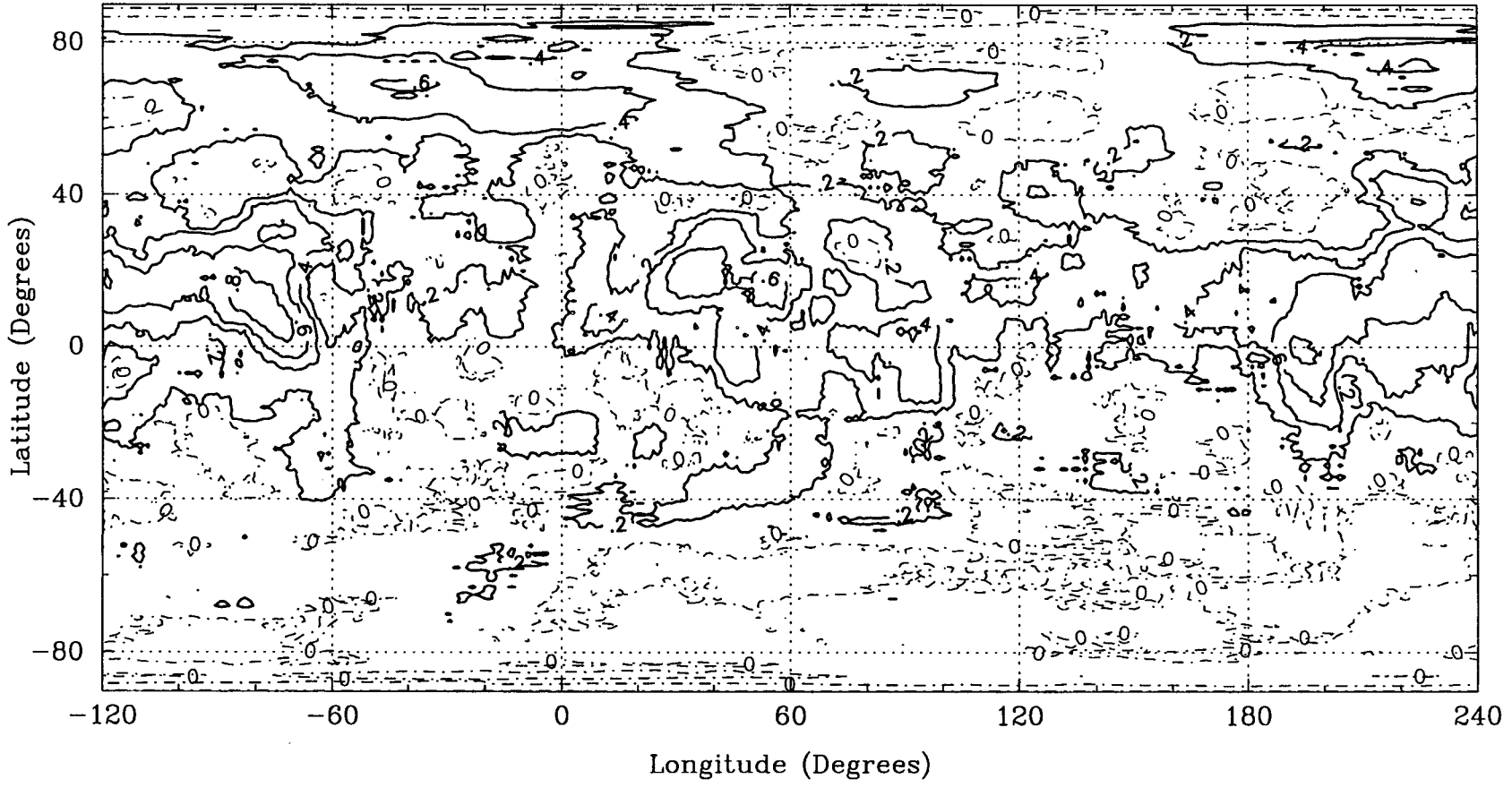
80
40
0
−40
−80
Latitude (Degrees)
−120
−60
0
60
120
180
240
Longitude (Degrees)

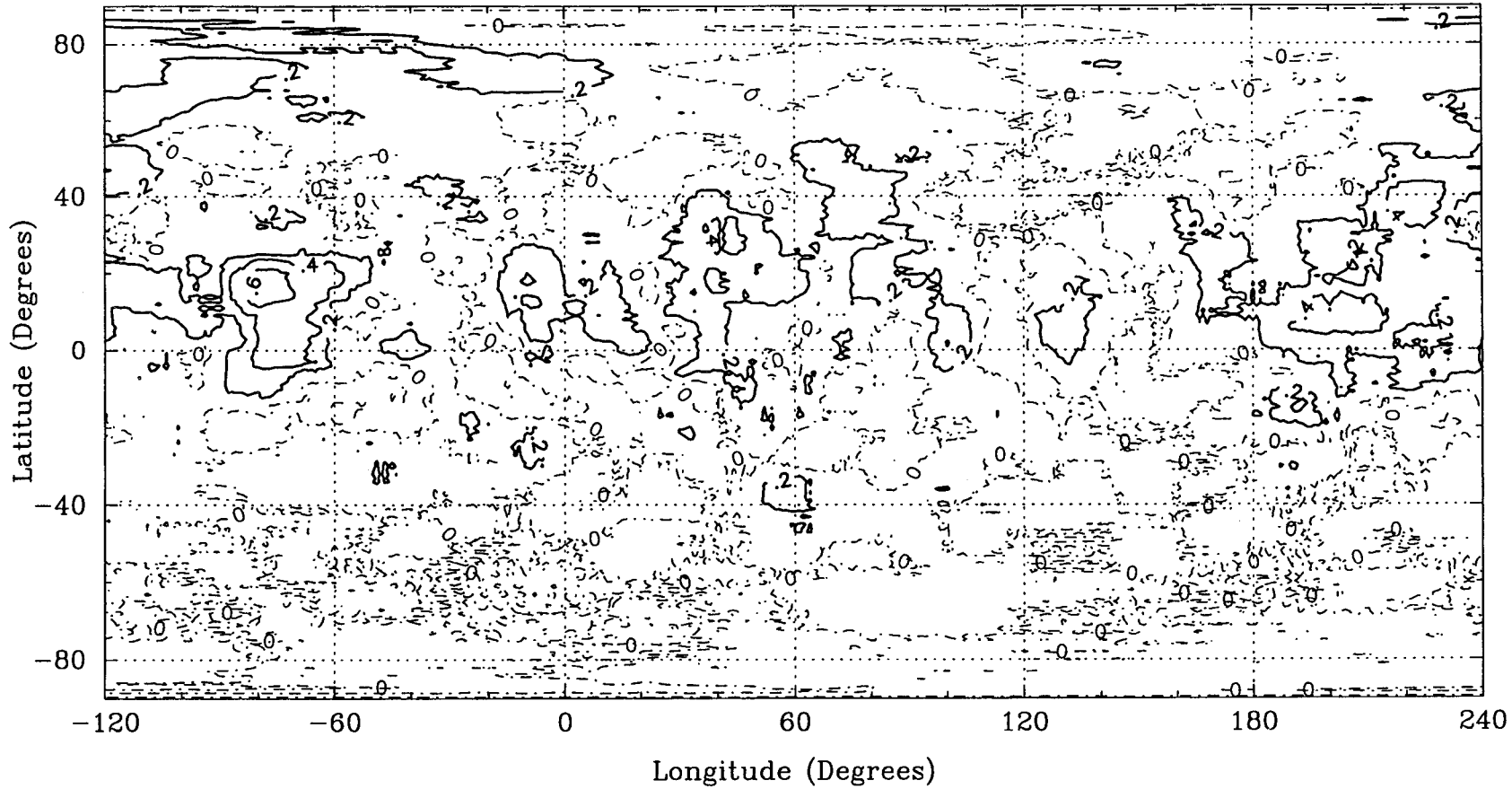
80
40
0
−40
−80
Latitude (Degrees)
−120
−60
0
60
120
180
240
Longitude (Degrees)

Fig 9